19784
P.27

324462

N95-14626

A Radio Telescope for the Calibration of Radio Sources at 32 Gigahertz

M. S. Gatti and S. R. Stewart
Ground Antennas and Facilities Engineering Section

J. G. Bowen and E. B. Paulsen
Radio Frequency and Microwave Subsystems Section

A 1.5-m-diameter radio telescope has been designed, developed, and assembled to directly measure the flux density of radio sources in the 32-GHz (Ka-band) frequency band. The main goal of the design and development was to provide a system that could yield the greatest absolute accuracy yet possible with such a system. The accuracy of the measurements have a heritage that is traceable to the National Institute of Standards and Technology. At the present time, the absolute accuracy of flux density measurements provided by this telescope system, during Venus observations at nearly closest approach to Earth, is ±5 percent, with an associated precision of ±2 percent. Combining a cooled high-electron mobility transistor low-noise amplifier, twin-beam Dicke switching antenna, and accurate positioning system resulted in a state-of-the-art system at 32 GHz. This article describes the design and performance of the system as it was delivered to the Owens Valley Radio Observatory to support direct calibrations of the strongest radio sources at Ka-band.

I. Introduction

NASA is planning to use the 32-GHz frequency band for communication and navigation of future deep space missions. Precise performance estimates of ground station capability are needed for both mission planning and technology development. To meet this need, a plan has been developed at JPL to determine with high accuracy the absolute gain of Deep Space Network (DSN) antennas.

At the present time, only estimates of the fluxes of celestial objects are available, since there have been no direct observations using highly calibrated telescopes, only extrapolations. A program that utilizes a 5-m-diameter radio telescope at the Owens Valley Radio Observatory (OVRO), operating at 32 GHz, is underway to observe a list of radio sources. If the gain of that antenna is accurately known, then the flux density of the sources may be accurately calculated. It therefore became necessary to calibrate the OVRO antenna to the highest accuracy possible. This article describes the instrument used to perform that calibration.

In order to minimize antenna-gain measurement error, we have developed a radio telescope intended to be a standard gain tool to measure the flux density of celestial radio sources. This telescope uses a highly efficient 1.5-m offset-feed Cassegrainian optics configuration. The aperture efficiency of this telescope

has been measured at nearly 80 percent. The telescope uses a radiometer with a high-electron mobility transistor (HEMT) low-noise amplifier (LNA) and a pair of feeds to operate in a beam-switching mode.

II. System Requirements

The stated goal of the 32-GHz calibration is to improve the accuracy of radio source flux densities from the present value of 20 percent (±0.8 dB) to 10 percent (±0.4 dB). However, in order to achieve a final result of this magnitude, the OVRO 5-m radio telescope that performs the direct observations must have knowledge of its gain to approximately 7 percent (±0.3 dB). Thus, any standard gain calibrator telescope total error must be able to calibrate the flux of a source to approximately 5 percent (±0.2 dB) total error.

JPL had a 1.5-m offset-feed Cassegrainian antenna left over from previous experimentation. Using this as the basis for our standard gain calibrator fixes many parameters. Specifically, the aperture size of the standard gain antenna is such that at 32 GHz, only the strongest radio sources can be used if a reasonable signal-to-noise ratio (SNR) is expected. We therefore expect the planet Venus to be the best calibrator. A plan was developed for simultaneous observations with both the OVRO 5-m antenna and the 1.5-m standard gain antenna during the summer of 1993, when that planet's approach was closest to Earth. Future articles will detail the results of those measurements.

The selection of a calibrator source and the desire to make 5-percent measurements allow one to calculate the SNR necessary for the system. In this case, it is expected that the measurement precision will be approximately 2.5 percent of the measurement, i.e., a radiometer SNR of 16 dB. In order to derive specific radiometer requirements, we define the minimum detectable signal of the radiometer, ΔT_{min}, and compare it with the expected flux of the source, in our case Venus. This minimum detectable signal is given by [1,2]:

$$\Delta T_{min} = \frac{2T_{sys}}{\sqrt{\tau B}} \tag{1}$$

where T_{sys} is the system operating noise temperature, τ is the system time constant, and B is the system bandwidth. The factor of 2 comes from the use of a Dicke radiometer where the source is observed for only one-half the time.

The signal part of the SNR will be in the form of an increase in system temperature of the radiometer signal when the system is pointed to the source, in our case Venus. The maximum possible signal that can be produced by a radio telescope is given by [1,2]:

$$\Delta T_{100\%} = \frac{SA_p}{2kC_r} \tag{2}$$

where S is the source flux in $\mathrm{Wm^{-2}Hz^{-1}}$, A_p is the physical area of the receiving antenna, k is Boltzmann's constant (1.38062×10^{-23} J/K), and C_r is the correction for sources that are not true points with respect to the antenna beamwidth. For the 1.5-m antenna, the source size correction factor C_r is never more than 1.001.

The equation for the SNR of our system can now be written

$$SNR = \frac{\Delta T_{100\%}}{\Delta T_{min}} \tag{3}$$

For the expected flux of Venus during the time of our calibrations (S = 950 Jy, where 1 Jy = Janskys = 10^{-26} $Wm^{-2}Hz^{-1}$) and a desired SNR = 16 dB = 40, one may calculate the radiometer minimum detectable signal required from Eqs. (2) and (3) to be 0.0152 K. This will put a strain on any radiometer at this frequency; however, by allowing a large bandwidth, a reasonable 1-sec SNR can be achieved. The expected system temperature of our 1.5-m telescope was 75 K, and the system hardware was operable over a 3-GHz bandwidth, limited mostly by the feedhorn. Therefore, when coupled with the required minimum signal, the selection of 3 GHz indicated that in 1 sec an SNR of 23 dB can be attained. This does not require herculean effort and provides a margin on the SNR for the real-world variations that often degrade the ΔT_{min}. As the signal is reduced due to Venus' increasing distance after April 1, 1993, the SNR will also decrease. This can be easily overcome by more averaging, i.e., integration time. Careful analysis of the standard deviations of the measurements will be required to assure that enough SNR is attained to achieve 2.5-percent measurement precision.

The pointing requirement on this system was developed as a result of the desire that there be no more than a 1-percent loss due to mispointing. This 1-percent loss translates to a beam-pointing error of no more than 0.03 deg. This error is split up between the feed support and the tracking-system tolerances.

The final requirement is on the type of radiometer itself. External effects of the environment, specifically the atmosphere fluctuations, are often on the order of kelvins. To achieve levels in units of millikelvins for the detected signal, a radiometer that is insensitive to external fluctuations is required. In order to overcome the problem of external fluctuations, a radiometric technique known as beam switching will be employed. This technique uses two antenna beams that sense signals on the sky at the same elevation but at different azimuths. By rapidly switching between the two signals and calculating the difference, one can infer the signal level of a source that is in one of the beams but not in the other. A summary of the performance requirements for the system is given in Table 1 below.

Table 1. Performance requirements for the standard calibrator telescope.

Parameter	Required value/type	Comment
Antenna size, m	1.5	Fixed
Signal SNR, dB	16	To provide 2.5% precision
Minimum ΔT, mK	0.0152	From SNR
Bandwidth, GHz	3	From SNR
Time constant, sec	1	May vary as required
System temperature, K	75	Desired best achievable
Total pointing error, deg	0.030	1% loss
Radiometer	Dicke BSR	Eliminate atmosphere

III. High-Gain Antenna

The requirement for having two secondary beams on the sky separated by a fixed angle in azimuth was met by employing two feedhorns that were laterally displaced from the focal point of the reflector system by a fixed amount. Microwave transmission lines (waveguides) then route the two signals to the Dicke circulator switch and on to the low-noise amplifier. This section describes the design of the antenna system, including the feed design, and the placement of the feeds with respect to the reflector focal point.

A. Antenna Description

The antenna used in this system consists of an offset-feed Cassegrainian reflector system, which is shown in Figs. 1 and 2. This type of configuration is also commonly called a clear-aperture antenna

system because there are no blockages due to feed and subreflector supports in the aperture of the antenna. Some of the advantages of this configuration are that it (1) allows for very precise and accurate analytical performance prediction, (2) eliminates the scattering and noise temperature effects common to feed and subreflector support struts, (3) provides higher efficiency systems, and (4) reduces sidelobe levels. A key advantage associated with the ability to make accurate performance predictions is that there is yet another way to eliminate concern regarding the calibration of the system as a whole.

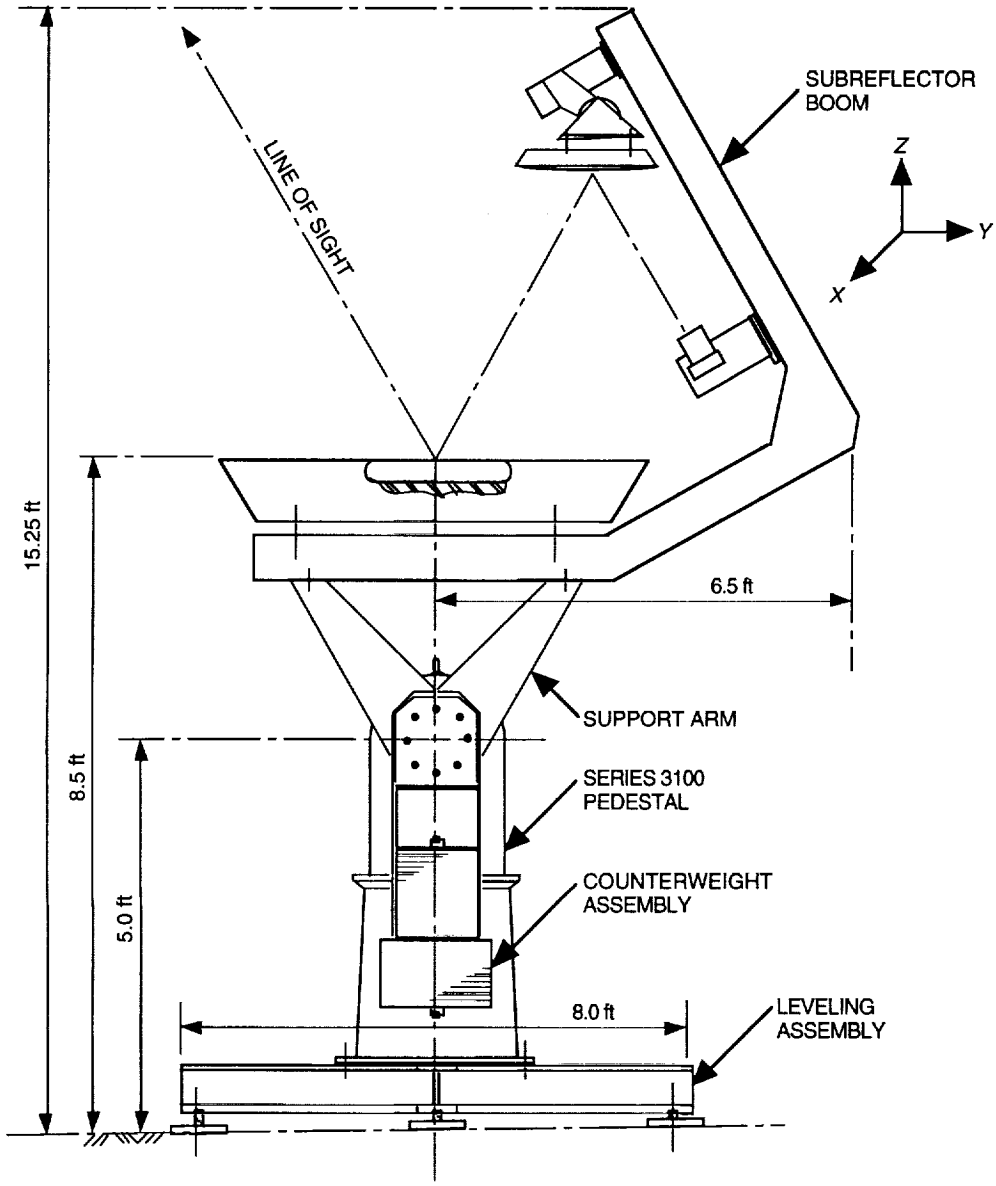

Fig. 1. The standard gain calibrator, 1.5-m diam.

The beamwidth of the antenna is defined by the size of the reflector and the feed pattern. For this system, maximum gain was primary, as the sidelobe levels would be minimized by the lack of aperture blocking in the system. The two antenna beams are reflections of each other about a vertical plane centered at the focal point of the reflector. They have the same beamwidths of 0.430 deg. The beams are separated from each other in azimuth by 1.0 deg and are at the same elevation angle for all positions of the antenna by using an elevation-over-azimuth positioner. The crossover point for each beam occurs on

the mechanical boresight of the antenna and is at a level of approximately −22.6 dB. Due to the electrical scanning of each beam, there are no significant sidelobes from one beam inside the other beam; however, on the opposite side of each beam, the first sidelobe level is −14.8 dB from the peak of the beam. The gain of the antenna at each feed input is 52.8 dBi.

Fig. 2. The reflector system.

B. Structure and Feed Supports

Since this system will be used as a standard with which measurements will be compared, the mechanical stability of the support structure is critical. Analysis was done to determine the maximum allowable deformations of the subreflector support due to gravity. This analysis was based on the requirement to have no more than a 0.025-deg beam-pointing error due to gravity distortions. The analysis used a baseline case of a feed that was placed in a Cassegrainian system with all mirrors exactly aligned. Parametric changes of the subreflector and feed positions were then input and subsequent performance calculations were made. The results of these calculations are shown in Figs. 3–6. Figures 3, 4, and 5 show the beam-pointing error for subreflector movement in the x-, y-, and z-directions, as defined in Fig. 1. Figure 6 shows the gain degradation of the system for motion of the subreflector in the z-direction.

Figures 7 and 8 show the beam-pointing errors for motions of the feed in the x- and y-directions. Note that for these analyses, the nominal case is for a feed that is placed at the focal point of the system, not the final configuration of the feed laterally displaced from the focal point, as required to develop the scanned beam on the sky. As a result of these analyses, the mechanical support for the feed and the subreflector were designed to be stiff enough to meet the requirements given in Table 2.

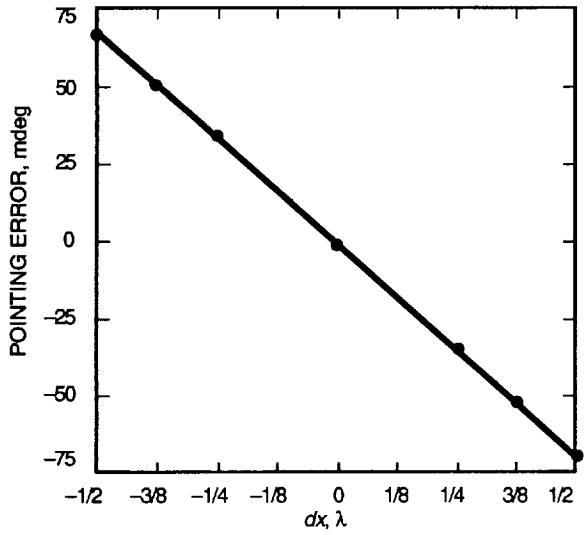

Fig. 3. Clear aperture antenna-beam pointing error due to subreflector movement in the *X* direction, *Y* polarized source, E_y field component, $\phi = 0$ deg.

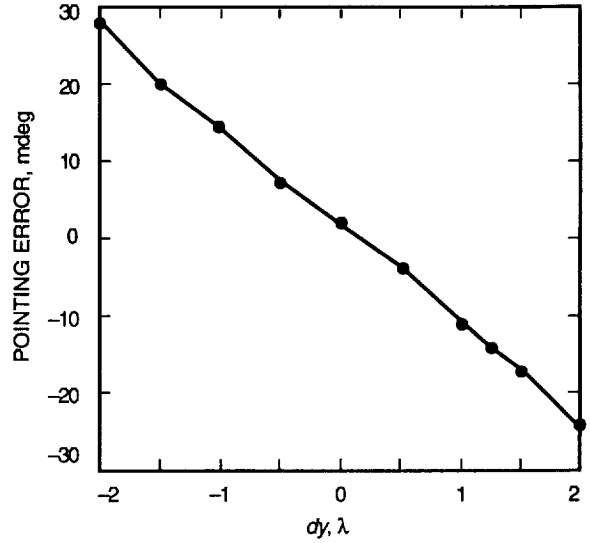

Fig. 4. Clear aperture antenna-beam pointing error due to subreflector movement in the *Y* direction, $\phi = 90$ deg, E_y field component, *Y* polarized source.

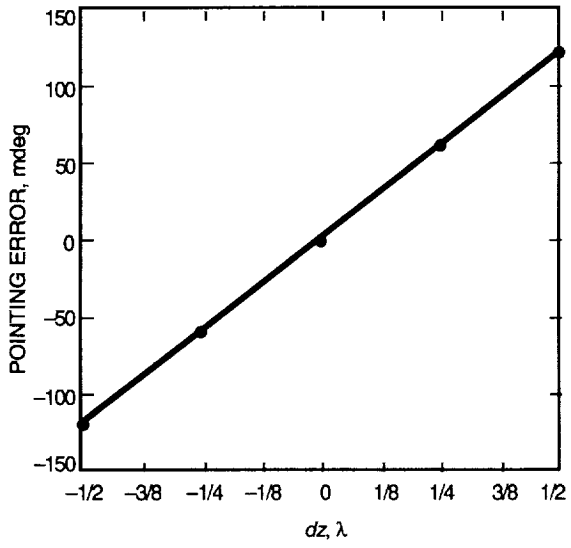

Fig. 5. Clear aperture antenna-beam pointing error due to subreflector movement in the *Z* direction, $\phi = 90$ deg, E_y field component, *Y* polarized source.

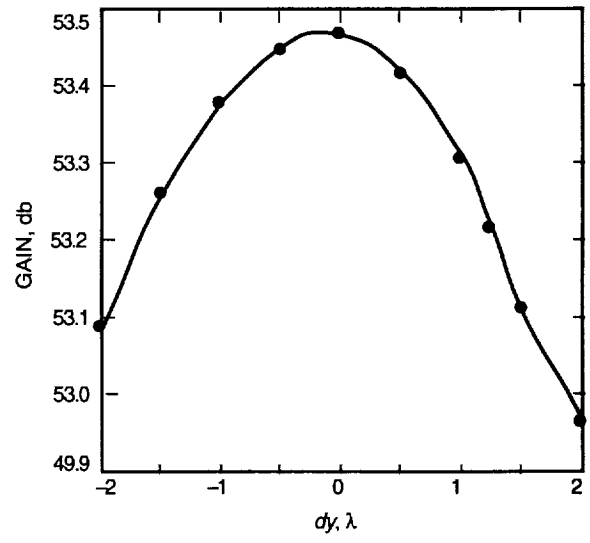

Fig. 6. Clear aperture antenna-gain degradation due to subreflector movement in the *Y* direction, $\phi = 90$ deg, E_y field component, *Y* polarized source.

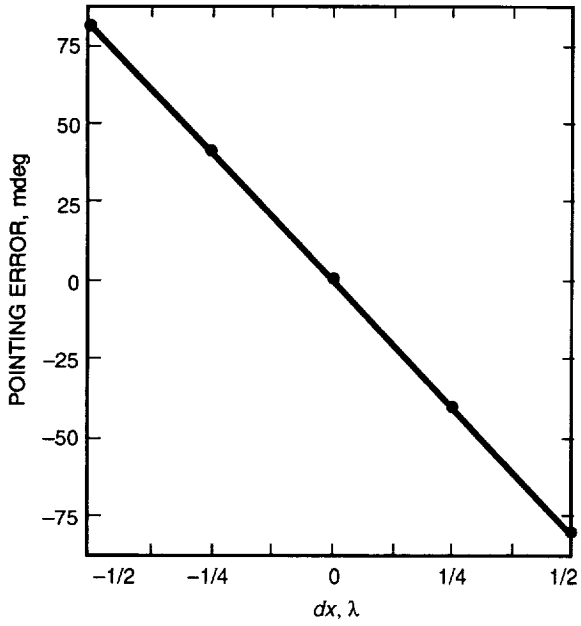

Fig. 7. Clear aperture antenna-beam pointing error due to source horn movement in the *X* direction, $\phi = 0$ deg, E_y field component, *Y* polarized source.

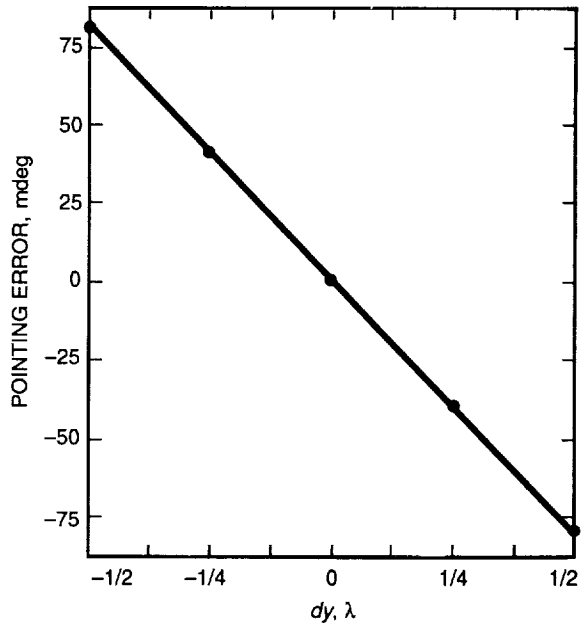

Fig. 8. Clear aperture antenna-beam pointing error due to source horn movement in the *Y* direction, $\phi = 90$ deg, E_y field component, *Y* polarized source.

Table 2. Mechanical tolerances for the motion of the subreflector and the feed system.

Direction of motion	Subreflector limits, λ	Feed limits, λ
Δx	±0.160	±0.135
Δy	±0.500	±0.140
Δz	±0.100	±0.250

C. Feed Design and Placement

The main reflector and subreflectors used in this system were inherited from a previous program commissioned to investigate the use of clear-aperture antennas for high-efficiency systems [3]. The focal length-to-diameter ratio, f/D, of the system had, therefore, been previously set. In order to obtain maximum gain, the feed must provide the proper illumination function, and for this system a 22.6-dBi gain feed is required. However, there is some choice of the type of feed that can be made to provide this illumination. For this system a Potter horn [4] was chosen. This horn typically provides ±5 percent bandwidth, or ±1.6 GHz, for a center frequency of 32 GHz, which is acceptable for the ±1.5-GHz bandwidth of the radiometer; however, it is the limiting factor in the system. The design of the feedhorn is shown in Fig. 9. This horn is circular in cross section and provides nearly uniform illumination in orthogonal planes due to its multimode aperture distribution. The generation of the two modes is done by the mode generator at the input of the horn, and proper phasing of the modes is accomplished by selection of the proper combination of the mode generator length and the step height of the horn input. These details are described by Potter [4].

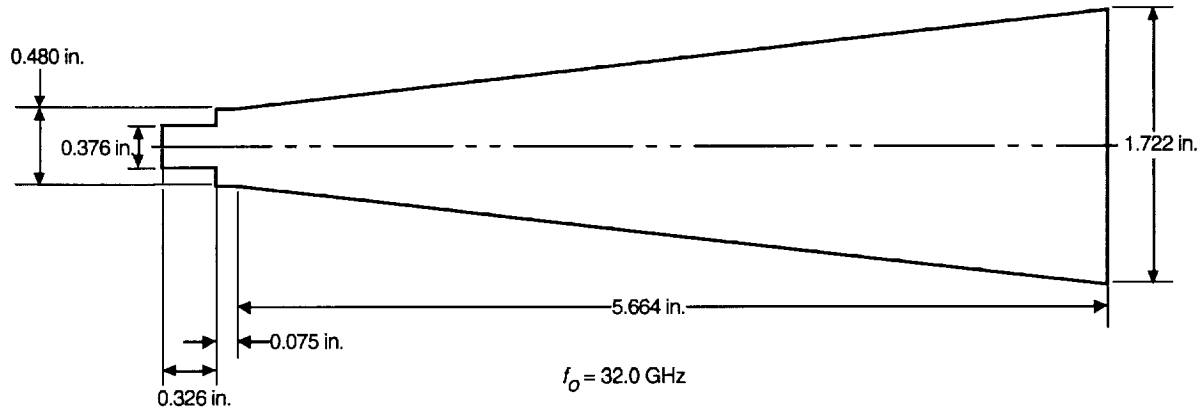

Fig. 9. Potter horn used as feed for 1.5-m antenna, G = 21.95 dBi.

By using the results of the previous tolerance analysis on beam scan versus x-axis motion (Fig. 3), one can calculate the required displacement necessary for providing a beam on the sky that is 0.5 deg off the mechanical axis of the antenna, so that each beam is 1.0 deg apart from the other. The slope of the line in Fig. 3 is 0.162 deg scan/λ displacement. Therefore, a 0.5-deg scan requires 3.09λ (= 2.90 cm) displacement in the x-direction.

A second concern regarded the axial placement of the feedhorn with respect to the focal point of the reflector system. All the analyses assumed properly focused feeds. As is typical with flared horns, the phase center of the horn is some distance behind the aperture of the horn. A parametric study was done to determine the position of the feed phase center. This was done by calculating the total antenna gain (excluding all losses) as a function of the feed axial focus position. The actual feed pattern calculated for this horn was used in the analysis. Figure 10 shows the result of that study, where all distances are given with respect to the aperture of the feed. The conclusion is that the optimum gain occurs when the feed is placed with its aperture 0.725 in. closer to the subreflector, i.e., the feed phase center is behind the feed aperture by that distance.

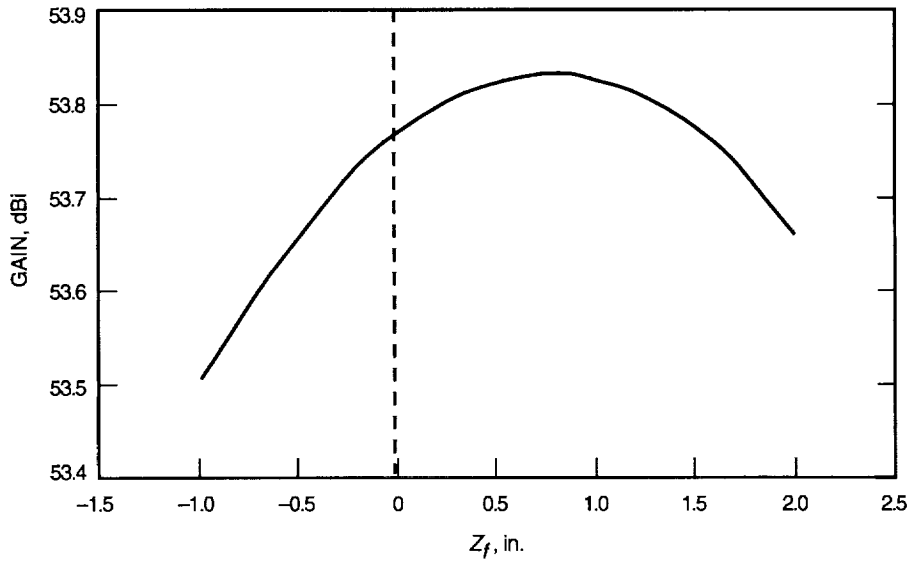

Fig. 10. Antenna gain as a function of feed placement. Position is given with respect to feed aperture; +Z is toward the subreflector.

Figure 11 shows the final configuration of the two horns used to develop the two antenna beams on the sky. To check this, a computer analysis of the antenna system was made in which the feed was displaced by 3λ (= 2.8 cm) from the focal point. For the 0.162-deg scan/λ displacement, the 3λ displacement should yield a scan of 0.486 deg. As seen in Fig. 12, the beam peak occurs at 0.483 deg off the boresight of the antenna—extremely close to what was predicted. This gives us good confidence that the model is accurate and that a 0.5-deg beam scan will be achieved by a displacement of 3.09λ (= 2.90 cm).

D. Performance Predicts

The performance predicts were done using a physical optics model of the antenna system. This model uses actual measured data for the main reflector and subreflector, both of which were shaped to provide the maximum possible efficiency. Furthermore, the pattern from a 22.6-dBi gain feedhorn was used as the illuminating source. This is the same model used for the analysis used to determine the mechanical tolerances for the structure described above. An analysis was done with the information regarding the feedhorn size, gain, and placement with respect to the phase center of the reflector system. The gain, beamwidth, and sidelobe predictions are based on the feedhorn being displaced by 3λ from the optical phase center of the reflector system. These results are shown in Fig. 12. Table 3 shows the predicted values of the parameters. The beam location is predicted by using the slope of the scan angle versus lateral displacement, as given by Fig. 3, and is defined to be 0.5 deg from the mechanical boresight. The beam scan of 0.5 deg for each beam implies that the separation of the beams is 1.0 deg.

Table 3. Performance predictions for the 1.5-m telescope.

Parameter	Prediction	NIST calibration
Antenna gain, dB		
Beam A	53.09	53.04
Beam B	53.09	52.96
Antenna efficiency, percent		
Beam A	80.6	79.7
Beam B	80.6	78.25
Half-power beamwidth, deg	0.430	0.430
Azimuth angle between beams, deg	1.0	1.0
Azimuth angle from beam to mechanical boresight, deg	0.5	0.5
Elevation angle between beams, deg	0	0.02
First sidelobe level, dB		
Beam A	−17	−15
Beam B	−17	−14
First sidelobe location, deg	0.58	0.625

E. NIST Calibrations

The fact that very accurate calculations of the system performance can be made does not relieve one from making independent measurements of the system, especially since the system will be used as a standard reference. Therefore, the antenna system and feeds were shipped to the National Institute of Standards and Technology (NIST) in Boulder, Colorado. The system was then characterized in the near-field facility for the parameters of interest, as described in the previous section. As part of the NIST calibrations, a method was devised to disassemble and then reassemble the system with extremely repeatable results. This method depended on placing retroreflectors on all the removable items: the subreflector, the main reflector, the support structure, and the positioning system. Tests at NIST proved that the antenna could be dismantled into its major components and then reassembled with no measurable changes in performance.

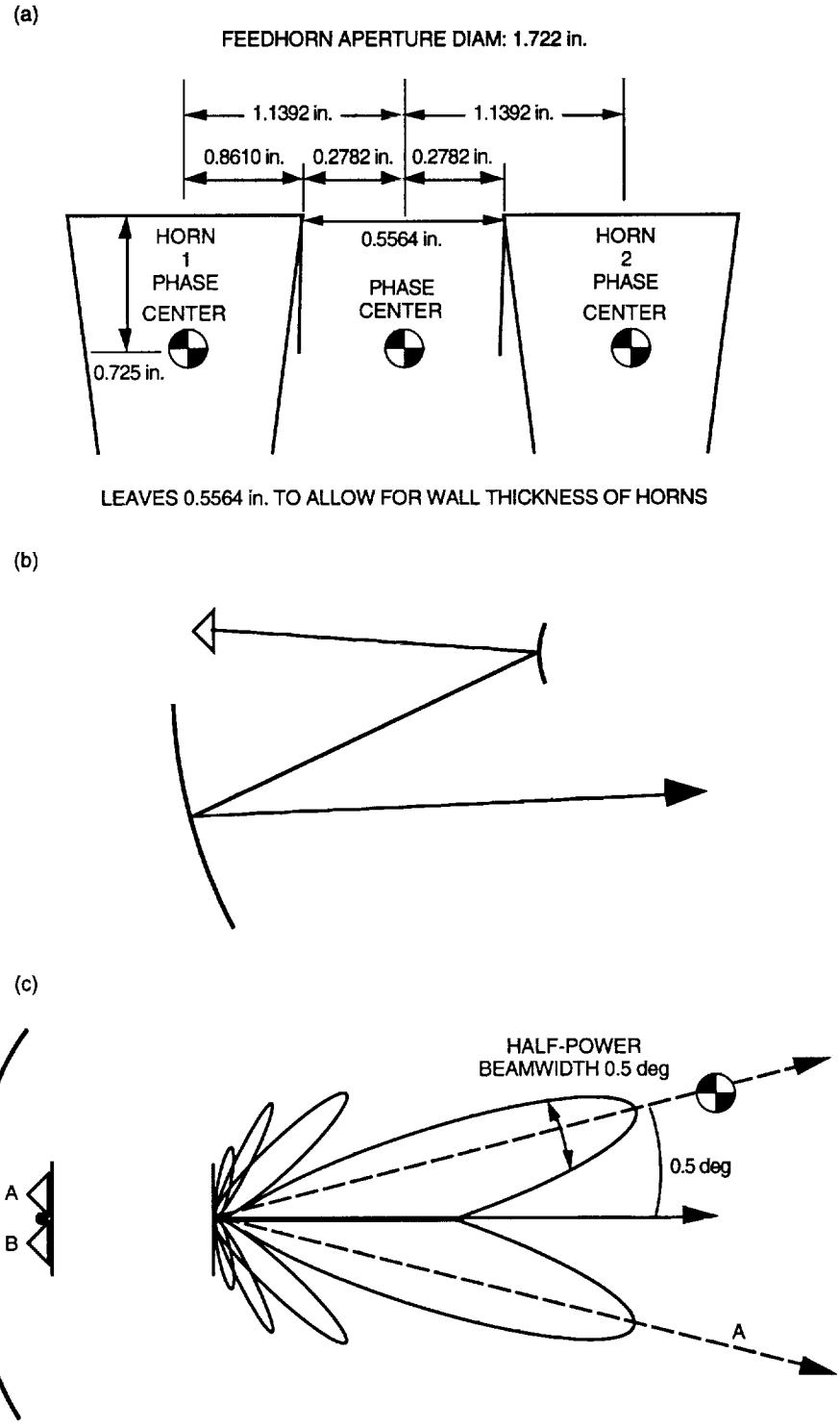

Fig. 11. Twin feedhorn layout to generate scanned antenna beams: (a) detailed layout showing the relationship between horn phase center and reflector system phase center; (b) sideview of the general layout showing the relationship between feeds, the reflector system, and antenna beams on the sky; and (c) top view of the general layout.

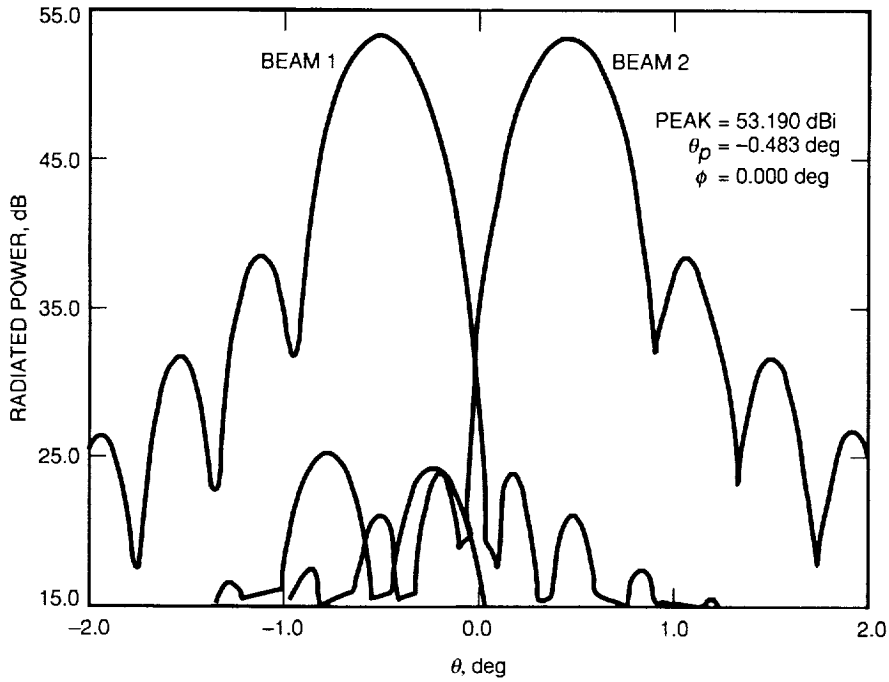

Fig. 12. Predicted telescope antenna patterns for feed lateral displacements of three wavelengths.

The system was characterized at three frequencies and at two elevation angles. The frequencies were at 31.8, 32, and 32.3 GHz. The two elevation angles were 0 and 22.5 deg. The purpose of the multiple elevation-angle measurements was to determine any possible gain dependency with elevation. The measurements did not indicate any measurable gain dependency with elevation, and the only gain dependency with frequency was accounted for by the theoretical expectations, i.e., by $1/\lambda^2$. The results are given in Table 3 and show a very good comparison to the predicted values, as described in the previous section. A typical pattern of the high-gain antenna is given in Fig. 13. Detailed results of the NIST calibrations may be found in [5].

IV. Radiometer Design

A. Radiometer Type

The radiometer to be used is a balanced Dicke radiometer [6], as shown in Fig. 14. Signals from the high-gain antenna are transmitted to the front end of the radiometer via either of two identical antenna beams on the sky. The term for this type of radiometer is a beam-switching radiometer. The radiometer includes a noise diode to perform both the sky signal calibration and radiometer linearity measurements. The front-end controller includes a switch to select one or the other of the two beams. All these items are contained within the cryogenic refrigerator. The back-end equipment consists of a single-stage, double-sideband downconverter that provides an intermediate frequency (IF) of 45–1700 MHz, a 1500-MHz filter, a square-law detector, a Stanford Research Systems SR-510 digital lock-in amplifier, and a square-wave generator. A computer is provided to control the entire system and to acquire and store the measured data.

B. Front-End Section

1. RF Components. The RF receiver consists of a cryogenically cooled 32-GHz high-electron mobility transistor (HEMT), a low-noise amplifier (LNA), and an ambient temperature follow-up amplifier. The LNA is mounted in a vacuum vessel with a closed-cycle refrigerator (CCR). This vacuum vessel is mounted on the antenna below the focal point.

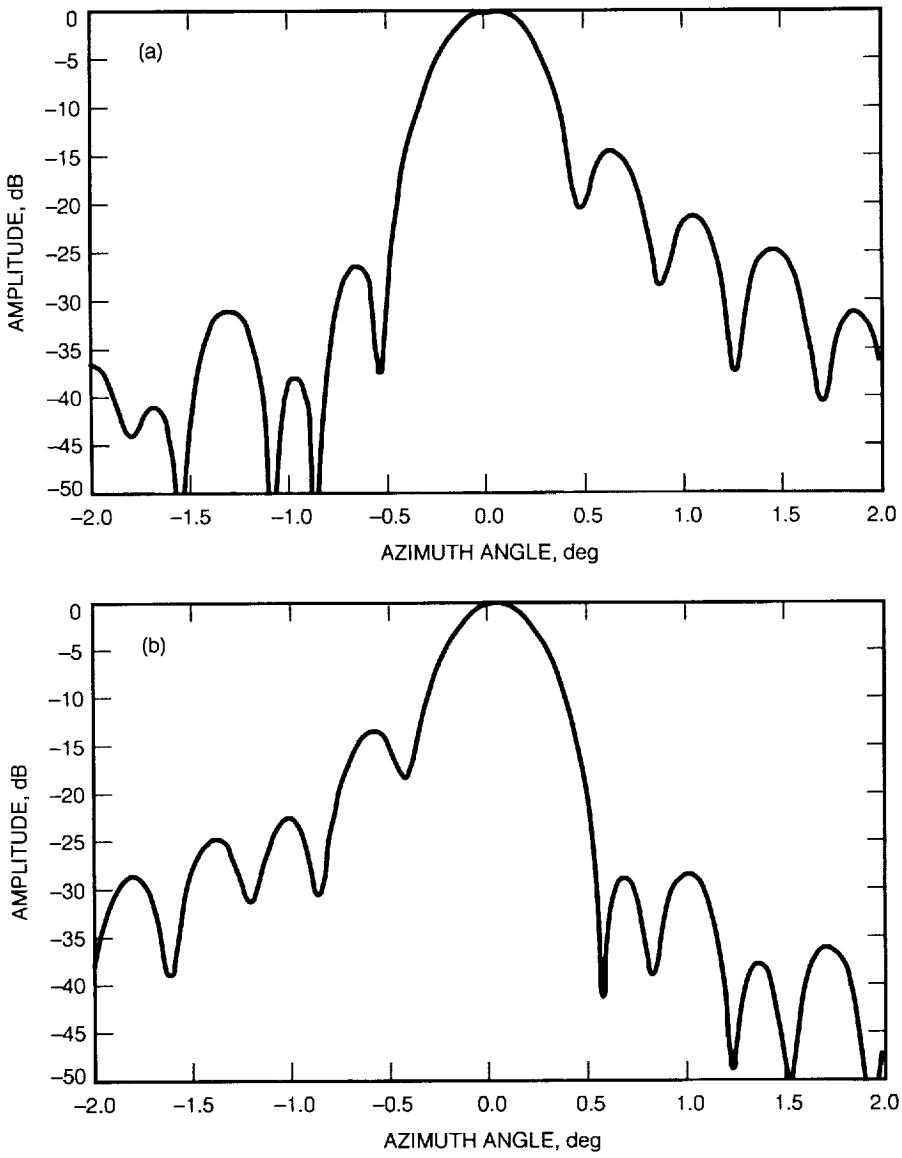

Fig. 13. Clear aperture antenna azimuth patterns as measured by NIST in the near-field facility: (a) beam A and (b) beam B.

The feeds and their associated mode generators, tapers, and vacuum windows are mounted to the top plate of the vacuum vessel. The top plate provides circular waveguide feedthroughs. Inside the vacuum vessel are waveguide sections that provide thermal insulation but are very low loss. This low loss is accomplished by using copper waveguide suspended in a fiberglass tube. The waveguide is only connected at the cooled junction, with the fiberglass tube providing the structural support [7].

Following the waveguide insulators are round-to-rectangular (WR-28) transitions that feed the microwave energy to hybrid polarizers. The left circularly polarized (LCP) port is terminated and the energy is tapped from the right circularly polarized (RCP) port. At this point, 30-dB waveguide crossguide couplers are placed in the signal paths, which allow signal injection from a noise diode that is located outside the vacuum vessel.

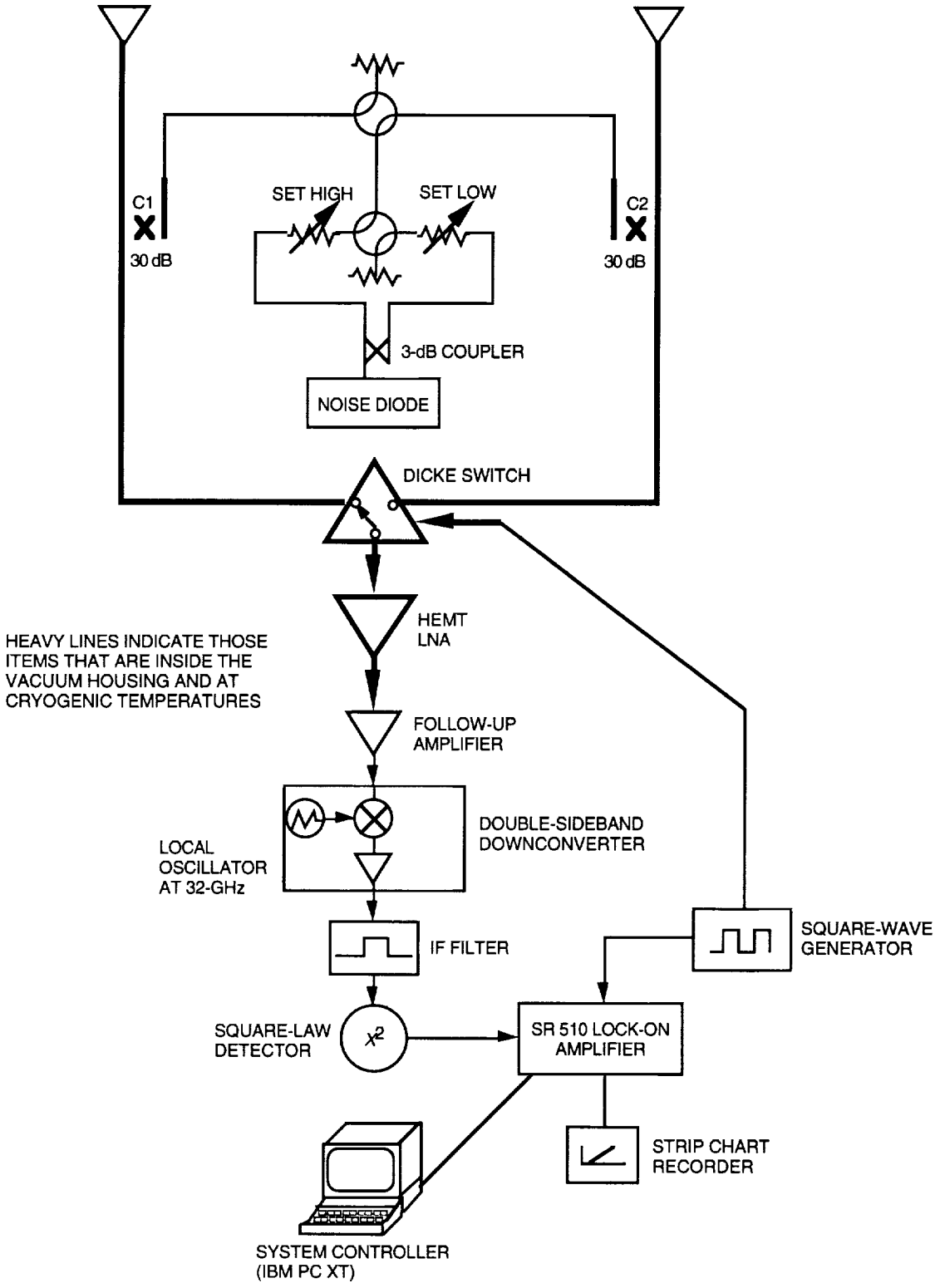

Fig. 14. The 32-GHz clear aperture antenna radiometer.

The outputs of the separate feeds are sent to a (Dicke) switching circulator. This switching circulator is a WR-28 circulator manufactured by Electromagnetic Sciences, Inc. It provides more than 20-dB isolation with less than 0.3 dB of insertion loss and is tuned for 32 GHz at a 77-K physical temperature. From the circulator, the selected feedhorn is coupled to the LNA input isolator. This isolator provides a consistent match for the LNA input while loss is less than 0.25 dB at 12 K.

The LNA is a four-stage amplifier built by the National Radio Astronomy Observatory (NRAO). This amplifier uses four Fujitsu FHX10X transistors in a single-ended design. At 32 GHz and 23 K, the amplifier provides 28 dB of gain at a 49-K noise temperature.

At the output of the amplifier is another isolator. The signal is then coupled out of the vacuum vessel through the bottom plate of the vessel using WR-28 waveguide.

2. Controls. Attached to the pedestal of the telescope is an instrumentation box. This instrumentation box has four major items: a servo power supply for the LNA, a vacuum gauge, a thermometer, and a control panel for routing power to all components and control of waveguide switches. In parallel with the control panel in the instrumentation box is a remote control panel in the control trailer that provides the operator with remote control over all receiver components. There is also a downconverter assembly box that is attached to the front end of the radiometer. This assembly contains the downconverter, a dc control assembly, and the noise injection assembly.

The dc control assembly contains a portion of the control relay switching and power conversion. Attached to this box is the Dicke beam-switching circulator control. This assembly derives its power and control from the dc control assembly. The switching circulator requires a very short, high-voltage pulse to change the field polarity of the circulator. This pulse is controlled by an assembly provided by Electromagnetic Sciences and only requires transistor–transistor logic (TTL) switching levels.

3. Noise Injection. Inside the downconverter assembly is a noise diode with an excess noise ratio (ENR) of 23 dB. Two waveguide switches are in series, which permits selection of one of two sources and selection of which input arm the source is coupled to. The noise diode is mounted to a proportional heater assembly to maintain a fixed temperature. A waveguide switch allows connection of the noise diode to either input feed. A second waveguide switch was incorporated to permit selection of a second signal injection source, if desired. This second port is normally terminated with an ambient 50-ohm waveguide load. The signal sources are transmitted out of the downconverter assembly and into the vacuum vessel in the WR-28 waveguide. Inside the vacuum vessel, the signal is routed to the cross-guide couplers, which are located in front of the switching circulator.

4. Cryogenics. The vacuum vessel consists of an aluminum tube 0.61-m tall with standard 0.20-m flanges at each end. All feedthroughs pass through the end plates. Mounted on the bottom plate is a CTI-Cryogenics model 350, two-stage, Gifford-McMahon refrigerator. This refrigerator cools the low-noise amplifier to 12 K. The refrigerator is driven by a model SC compressor from the same manufacturer. The top plate of the vacuum vessel has bolted to it a housing that covers the feedhorns. This housing has a Kapton window in its top and is charged with nitrogen to prevent condensation. Inside the vacuum vessel, surrounding the microwave components, is a thermal radiation shield, which is kept at 70 K by the first stage of the refrigerator.

5. Performance. As measured by NRAO, the amplifier (serial no. A11) exhibited a gain of 28 dB and a noise temperature of 48.4 K at 32 GHz and a 23-K physical temperature, referenced to the input of the amplifier. After installation in the radiometer, noise temperature was measured with reference to the input feedhorn and was 59.8 K. The physical temperature of the amplifier in this test was 17.6 K.

C. Intermediate Frequency

1. Downconverter. The downconverter assembly is underneath the vacuum vessel. The output from the vacuum vessel runs down through a waveguide filter and into the downconverter box. The signal

is amplified by an Avantek 32-GHz amplifier and coupled to a Watkins-Johnson mixer/YIG oscillator assembly and converted to the IF of 0–1700 MHz. This IF is then passed through a 1500-MHz low-pass filter. The filtered IF then is routed to the control trailer approximately 30 m away by a 7/8-in. hard line, where it is detected by the appropriate detector, as described below.

2. IF Path Performance. There were choices to be made with respect to locating the IF detector. The desire was to detect the IF as close to the downconverter as possible so as to minimize losses and other possible interferences. The detector was, therefore, placed in the downconverter assembly on the output of the low-pass filter. The first hint of a problem occurred when the system stability was found to be unacceptable. This problem was traced to the temperature variations of the detector as the ambient temperature changed. The first attempted fix was to temperature-stabilize the detector by placing it onto a heater unit. There were still problems with this, as the ambient temperature could change from 0 to 25 deg C in the course of a spring-type day at OVRO. We then decided to place the detector in the trailer, where the ambient temperature swings were controlled by the trailer heating and cooling system to ±3 deg C. The detector was further wrapped in foam to minimize any residual changes in its temperature. The 7/8-in. hard line between the trailer and the antenna was selected in order to minimize the loss versus frequency of the IF signal between the control trailer and the antenna. Figure 15 shows the IF path performance of this system. The curves show the IF loss versus frequency at the output of the low-pass filter on the antenna and at the output of the hard line in the trailer. For reference, the output of the IF is also shown in the case where standard RG59 coaxial cable is used. It is obvious that the hard line essentially brings the IF into the trailer with very little attenuation.

D. Detection

The block diagram in Fig. 14 shows that there are two methods to perform radiometry: in total power mode and in beam-switching mode. While beam switching is the method used during the actual tracking of sources, the total power mode is necessary to determine system performance, noise diode level, linearity, and atmospheric loss. These two modes are described in more detail in this section.

1. Total Power Mode. In total power mode, the IF is switched into the HP 438A power meter. Further, the switching circulator, here called the Dicke switch, is latched into one position. The position is chosen by the operator and the proper control switches are set to cut the square-wave generator out and set the Dicke switch to the desired position. Once this is done, the computer is then run as a total power radiometer, as described in many recent works [8,9].[1,2] The detector for this mode, an HP 438, is not the same as for the beam-switching mode; however, we would occasionally also employ an HP 3457A multimeter and use the same detector as used in the beam-switching mode to determine the system stability and linearity using that detector. This gave confidence in the system used during the beam-switching mode.

2. Beam-Switching Mode. The beam-switching mode of radiometry used for radio source observations has been described in several references [10–12]. The beam-switching mode is shown in Fig. 14, where the controls are set so that the square-wave generator provides the signal to the switching circulator and to the lock-in amplifier. The configuration of the circulator switch control, IF detection, square-wave generator, and lock-in amplifier are very closely related to the system described in [10]. A brief summary of how this system works follows.

---

[1] C. T. Stelzried, *Microwave Radiometer Calibrations*, JPL D-10496 (internal document), Jet Propulsion Laboratory, Pasadena, California, January 29, 1993.

[2] L. J. Skjerve, *Preliminary Documentation of DSS-13 Radiometer Program*, JPL D-9292 (internal document), Jet Propulsion Laboratory, Pasadena, California, January 1990.

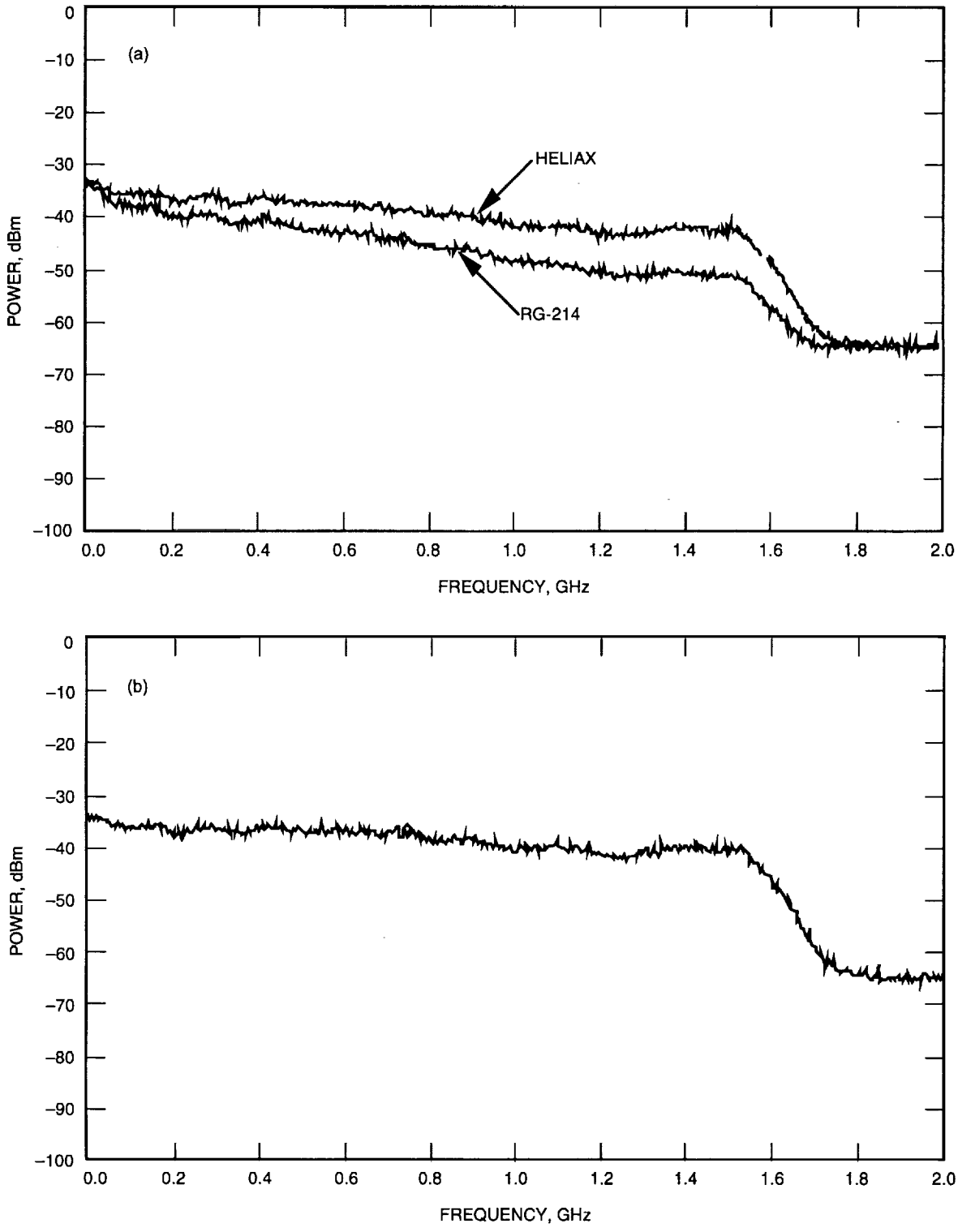

Fig. 15. Performance of the IF loss versus frequency between the antenna and the control trailer: (a) the IF signal as transmitted versus RG-214 to the control room, and (b) signal measured at the antenna pedestal.

The signal from the Dicke switch is a modulated square wave, the amplitude of which is the difference between the signals in the two beams. The lock-in amplifier demodulates this signal and produces the desired amplitude signal level. The computer is connected via a parallel data bus Hewlett Packard

interface bus (HPIB) to the lock-in amplifier. During the beam-switching mode, digital data are taken and a screen is generated that plots the difference signal as a function of time. If each antenna beam is observing the same target, such as the sky, and if the system is perfectly balanced, a zero signal from the lock-in amplifier will be recorded. When beam A is pointed to a radio source and beam B is off the source, the signal is proportional to the increase in system temperature due to the radio source. The output from a diode noise source is coupled into the waveguide of both beams and calibrates the system. The diode calibration was routinely switched on many times each hour as the radio sources were observed. With this procedure, the increase in system temperature produced by each radio source is calibrated and the adverse effects of gain variations in the HEMT and receiver are virtually eliminated.

E. Calibration

The calibration of the radiometer system is second in importance after the high-gain antenna calibration. Unlike the antenna-gain calibration, however, the radiometer calibration is done much more frequently. These calibrations quantify systematic errors and reduce random errors. Furthermore, the calibration of the system is done in both the total power mode and in the beam-switching mode.

In order to discuss the calibration of the radiometer, some quantities need to be defined. Specifically, the quantity that the radiometer measures is the operating system temperature, T_{op}. All other quantities are derived from this basic measurement, depending on the target that is in the beam of the high-gain antenna during the measurement.

The Institute of Electrical and Electronics Engineers (IEEE) definition of T_{op} is given by [13]

$$T_{op} = T_a + T_e \tag{4}$$

where T_a is the effective antenna temperature of the system looking towards the target at the reference plane where the measurement is defined, and T_e is the effective receiver temperature of the system looking towards the receiver at the reference plane where the measurement is defined. In our system, the following definitions are used:

T_{op} = operating system temperature

T_a = effective antenna temperature

T_e = effective receiver temperature

T_{sky} = temperature due to the sky contribution

T_{atm} = temperature due to the atmosphere

T_{gal} = 3.0-K cosmic background radio emission

T_{so} = temperature due to feed spillover

Furthermore,

$$T_a = T_{sky} + T_{so} \tag{5}$$

$$T_{sky} = T_{atm} + T_{gal} \tag{6}$$

The types of calibrations done in each mode, the purpose of each calibration, and the technique used to perform the calibration are described below.

1. Total Power Mode. Receiver Calibration. The receiver calibration is done to determine the effective receiver noise temperature, T_e, of the system.[3,4] This measurement is important because the receiver noise temperature is assumed to be known in the remainder of the total power radiometer calibrations. This quantity consists of the noise temperature of the transmission lines between the feeds and the LNA, the LNA contribution, and the contribution of the equipment connected to the LNA. The aperture load technique was used in these measurements. A single receiver calibration consists of from 5–10 individual measurements of the system, providing an average and statistics to determine the validity of the data. The details of this measurement technique are described in [10] and are not repeated here. Normally, this quantity does not change over time by more than a few percent. Nevertheless, since the absolute accuracy of the calibrations is paramount, this measurement is done biweekly during observation times.

Total Power Radiometer Calibration. The measure of T_{op} done by the total power radiometer has been extensively described earlier [8,9,14].[5] The system developed here calculates radiometer constants a_p, b_p, a_c, b_c, and c_c from a precalibration. The a_p and b_p constants are calculated for the case of a radiometer with a linear response. For the radiometer that has some active element in the beginning of its saturation curve, a nonlinear analysis results in the calculation of constants useful in providing corrected values of T_{op}. For this case, one needs to calculate the T_{op} from the linear analysis and then apply the nonlinear analysis coefficients a_c, b_c, and c_c. This is summarized by

$$T_{op} = a_p + b_p(P_m) \tag{7}$$

$$T_{op(nl)} = a_c + b_c(T_{op}) + c_c\left(T_{op}^2\right) \tag{8}$$

where the form of Eq. (8) is used when the linearity of the system as defined below is greater than 1.5 percent.

The precalibration consists of measuring the total noise power of the system while the antenna observes different targets. The targets are an ambient aperture load and the sky. Additionally, these measurements are done for two states of the noise diode: on and off. The information that results from these measurements yields not only the radiometer constants, but also the linearity of the system and the noise diode level. The system then performs repeated measurements of the system power, P_m, while applying the radiometer constants to yield T_{op}.

Radiometer Linearity. As mentioned earlier, a linearity metric of the system is a byproduct of the radiometer calibration. This linearity metric is the ratio of the noise diode level in kelvins, as measured while on the ambient load, $T_{nd(load)}$, and while on the sky, $T_{nd(sky)}$. This is written as

$$F_l = \frac{T_{nd(sky)}}{T_{nd(load)}} \tag{9}$$

It is important that only linear results are used in the measurement of radio sources in order to eliminate this effect from the list of possible systematic error sources. During the course of an observation track,

[3] C. T. Stelzried, op. cit.

[4] L. J. Skjerve, op. cit.

[5] C. T. Stelzried, op. cit.

a set of precalibrations will be periodically done to track this factor (along with the gain and the noise diode calibration). Figure 16 shows a plot of the linearity factor as a function of time during a track done in the summer of 1993.

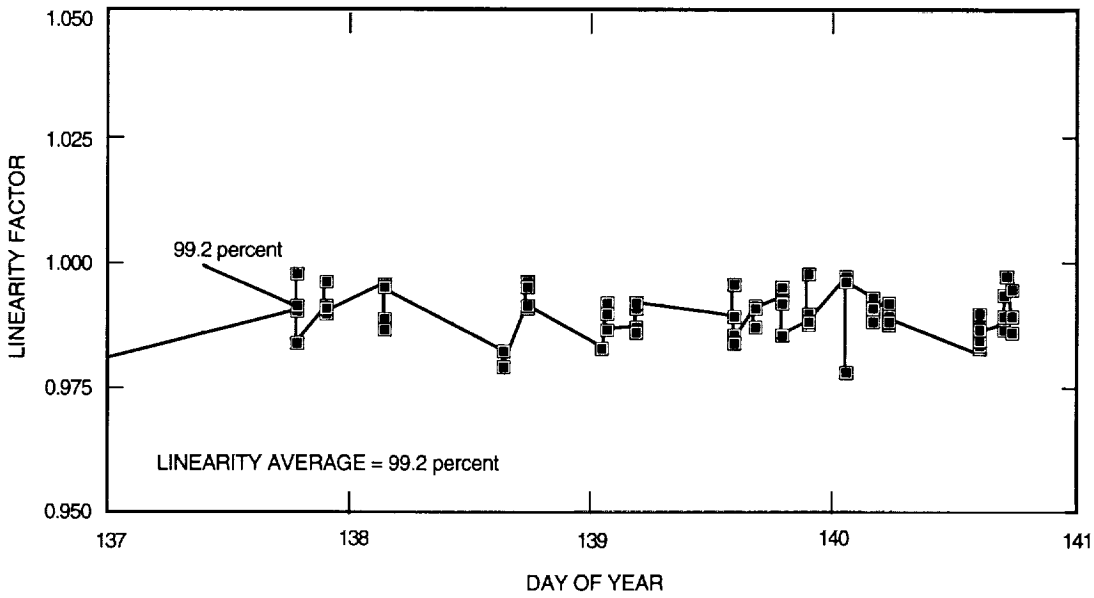

Fig. 16. Clear aperture system linearity for days 137–141 of 1993.

Noise Diode Calibration. Possibly the single most important calibration of the radiometer system is that of the noise diode. The level of noise temperature introduced by the noise diode to the system is critical because it is used to scale the final calibration of the radio-source temperature measurement. The calibration of the noise diode in the total power mode differs from the noise diode *measurement* performed while the radiometer is in the beam-switching mode, as described below. For this calibration, the radiometer constants are calculated as described above, and then the antenna is pointed to the zenith. The radiometer program is then capable of switching the diode on and off successively for a number of times selected by the operator. This number of times was generally chosen to be 15. The noise temperature was measured for each state of diode. The noise diode level was then calculated from the difference in the two system temperature measurements. It is thought that this is the most accurate method for calibrating the noise diode, since the time taken to perform the measurement is on the order of 2 min. For this time frame, the stability of the radiometer would be good and there could be little or no effect due to gain changes in the electronics. Other methods that could be used to calibrate the noise diode level include the measurement of the diode that is a byproduct of the linearity measurement described above; however, that measurement uses several targets and takes a considerably longer time to perform.

Radiometer Stability. For completeness, the stability of the radiometer was checked. The stability was measured while the ambient load was placed over the aperture of the feeds. The radiometer program then measures the load temperature, the system temperature, and noise diode levels. The system gain is calculated from

$$g = \frac{P}{kT_pB} \tag{10}$$

where the measured power on the ambient load is P, the temperature of the ambient load is T_p, the bandwidth of the system is B, and k is Boltzmann's constant. These data are written to files for postanalysis.

Figure 17 shows the results of a stability run. Shown are the gain and physical temperature. The stability of the system was used to define the time between the noise diode calibrations done during observations in the beam-switching mode as described below. For these measurements, a 10-min period between noise diode calibrations was considered conservative enough for our accuracy requirements. Furthermore, a 1.5-hr time frame was chosen to perform all the system calibrations for linearity, gain, and atmospheric effects.

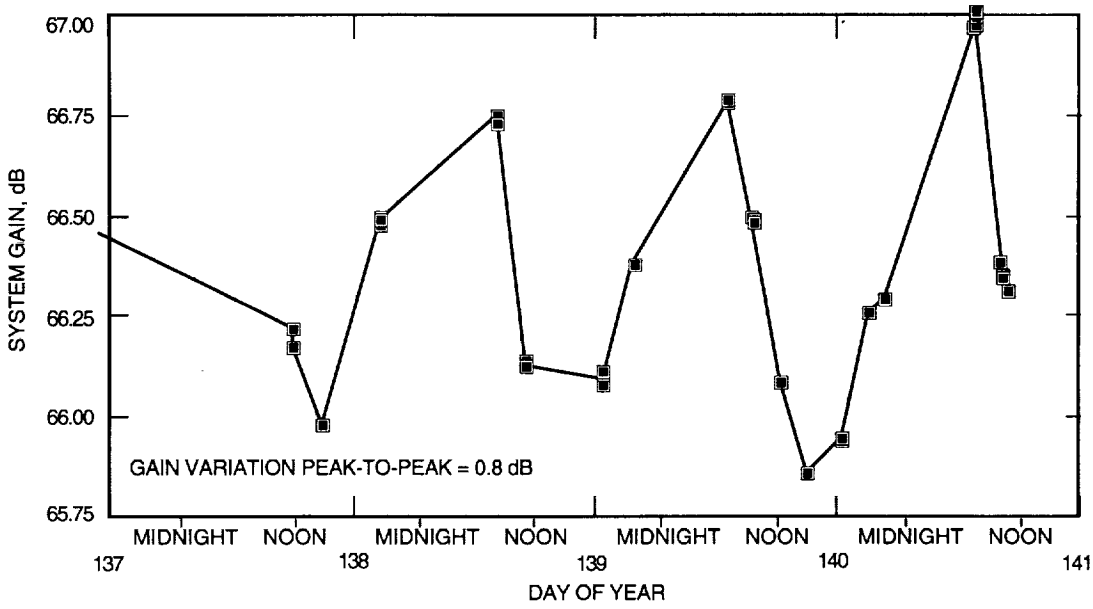

Fig. 17. Clear aperture system gain stability for days 137–141 of 1993.

Tipping Curves. The effects of the atmospheric attenuation to a received signal must be removed in order to correctly calculate either the antenna performance (gain) or the source flux. The most common method to predict the atmospheric effects is to measure the total system temperature as a function of elevation. The measured data can be used to calculate the zenith attenuation. This attenuation can then be used to calculate the attenuation as a function of elevation. The radiometer for this system included an option to perform such measurements and to store the data in files for future analysis. The data can be analyzed in any fashion desired by the observer. Furthermore, if a secondary measurement capability is available, such as a water vapor radiometer, it may be prudent to use it as the primary indication of the atmosphere with the antenna-tipping curves as backup. Figure 18 shows the results of a typical tipping curve. These data are shown as system temperature versus air mass, where the air mass quantity is defined as the amount of air relative to the zenith. At zenith, air mass is defined as 1. At lower elevation angles, the air mass increases. The relationship between air mass at an elevation angle is given by

$$air\ mass = \sec\ (90 - \theta_{el}) \tag{11}$$

The data are plotted in this way so that, to the first order, one can infer the noise temperature contribution due to the atmosphere (T_{atm}) as the slope of this line in kelvins/air mass. There are second-order effects that may be included in more thorough analyses, but they have been omitted here for simplicity.

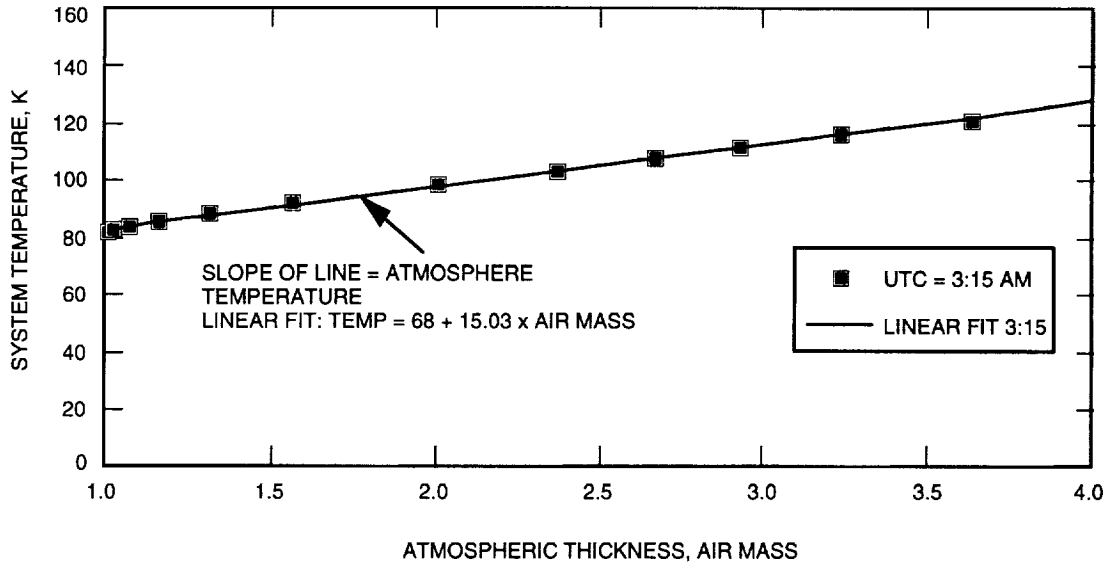

Fig. 18. Tip curve by CAA at OVRO: day of year 138.

The relationship between the noise temperature of the atmosphere, T_{atm}, and the loss of the atmosphere is again simply related as if the atmosphere were an attenuator in the radiometer. This relationship is given by

$$attenuation\ factor = \frac{1}{(T_{atm}/T_p) + 1} \tag{12}$$

where the physical temperature of the atmosphere is given by T_p and can be estimated in a number of ways from other observations, including surface meteorology. Typically, T_p is on the order of 240–270 K. All measured values of flux of a source would be divided by this attenuation factor (< 1) to correct for the loss of the atmosphere.

2. Beam-Switching Mode. Boresight Pointing Calibration. When an antenna is pointed at a source's expected azimuth and elevation, there is often an error due to gravity, refraction, azimuth and elevation constant offsets, and azimuth and elevation misalignments, and so there are tracking system errors. A systematic pointing-error correction model for determining a target's true azimuth and elevation from indicated azimuth and elevation must be generated to accurately point the antenna. In order to do this, several days must be spent scanning the antenna beam through radio sources at various right ascensions and declinations and comparing their actual positions with their indicated positions. To reduce the tedious aspects of this task, an automatic boresighting routine was incorporated into the antenna-tracking software. Details of the antenna-tracking system are discussed in the next section. The automatic boresight routine commands the antenna to track assorted points offset from the calculated center azimuth and elevation of the source and to record average power levels at those points with the radiometer in the beam-switching mode. By defining the offset points along the cross-elevation and elevation axial lines, pointing-correction tables become much easier to produce. Therefore, a software routine was developed to track five points along each axis: the 3-dB and 1-dB offset points on each side of the main lobe and the on-source point. At each of these points, the radiometer records a 20-sec average power level, and after each five-point scan, the software fits a second-order curve through these data points and calculates the pointing offset to the maximum power point on the curve. This pointing offset is then recorded and used to adjust the offsets in the subsequent scan.

By alternately scanning the cross-elevation and elevation axes and recording the accumulated pointing corrections in each axis for various radio sources in all quadrants of the sky, a pointing model was produced that corrected for fixed azimuth and elevation offsets, north/south and east/west azimuth tilt, and gravity and refraction distortions. When these values were then used in subsequent tracks to correct the azimuth and elevation coordinates, the antenna was able to achieve a blind-pointing accuracy of better than 0.02 deg. This is the total pointing error and is significantly less than the 0.03-deg requirement stated earlier.

The pointing model generated was developed using the antenna beam referred to as beam A. After this model was made, tracks of radio sources were done for the antenna beam referred to as beam B. The result of these tracks indicated that the two beams were 1.0 deg apart in azimuth and 0.015 deg different in elevation, indicating excellent agreement with what was measured in the near-field measurements described above.

Flux Measurements. The term "flux measurement" in this section refers to the measurement of the system response in volts due to the increase in system temperature of a source located on the boresight of either antenna beam. Furthermore, what is actually measured is the increase in system temperature in kelvins due to the source. However, until properly scaled by an associated noise diode measurement, given as kelvins/volts, this value is not yet in units of kelvins. The actual flux of the source in Janskys is calculated after the measurement with knowledge of the antenna gain, given by an equation similar to Eq. (2).

Flux measurements are made by observing the signal of the source while it is sequentially presented to both antenna beams. For this discussion, we refer to the beam on the sky providing a signal to its associated feedhorn. Also recall from the discussion above regarding detection in the beam-switching mode, that the signal from the lock-in amplifier is zero for the case when there is no signal in either beam. Furthermore, the signal in beam A differs in sign from a signal in beam B due to the detection method of the lock-in amplifier. With this information, flux measurements can be made and understood.

With the receiver in the beam-switching mode measuring the difference between the signal levels in antenna beams A and B, the antenna is moved so that four measurements could be made with the signal from the radio source focused on feeds B, A, A, and B. The sum of the feed B measurements (a negative value) was subtracted from the sum of the feed A measurements, and the result was divided by four to obtain an average source signal level. The resulting value is a measure in volts of the system response to the source.

All this information is acquired as digital data and is stored in files for further analysis. The computer screen also plots the information in graphical format for the operator to observe. This is often useful in determining if the data are high-precision or not, i.e., clean. A representative example of this display is given in Fig. 19. The larger signals at the beginning of the chart are noise diode signals, as described below. For reference, the noise diode signal is approximately 0.75 K.

Noise Diode Measurement. In order to conduct accurate flux measurements, gain drifts in the receiver must be calibrated out. These calibrations were accomplished throughout the tracks by periodically injecting the signal from a well-calibrated and stable noise diode into the receiver RF path of horn A and measuring the change in detected power level. Since all other variables in the system can be taken as constants during the short calibration period and the effects of atmospheric noise contributions are eliminated in the beam-switching mode, the change in detected power level from the diode is due only to long-term receiver gain variations. The system response due to the injection of the noise diode is measured in volts. With knowledge of the noise diode level, from the total power noise-diode calibrations, one can calculate the scaling factor of the injection signal in kelvins/volts. This measurement is done at the beginning and end of each flux measurement described above. Therefore, system gain drifts on the order of 5 min are continually monitored and the data are used in the calculation of the source temperature.

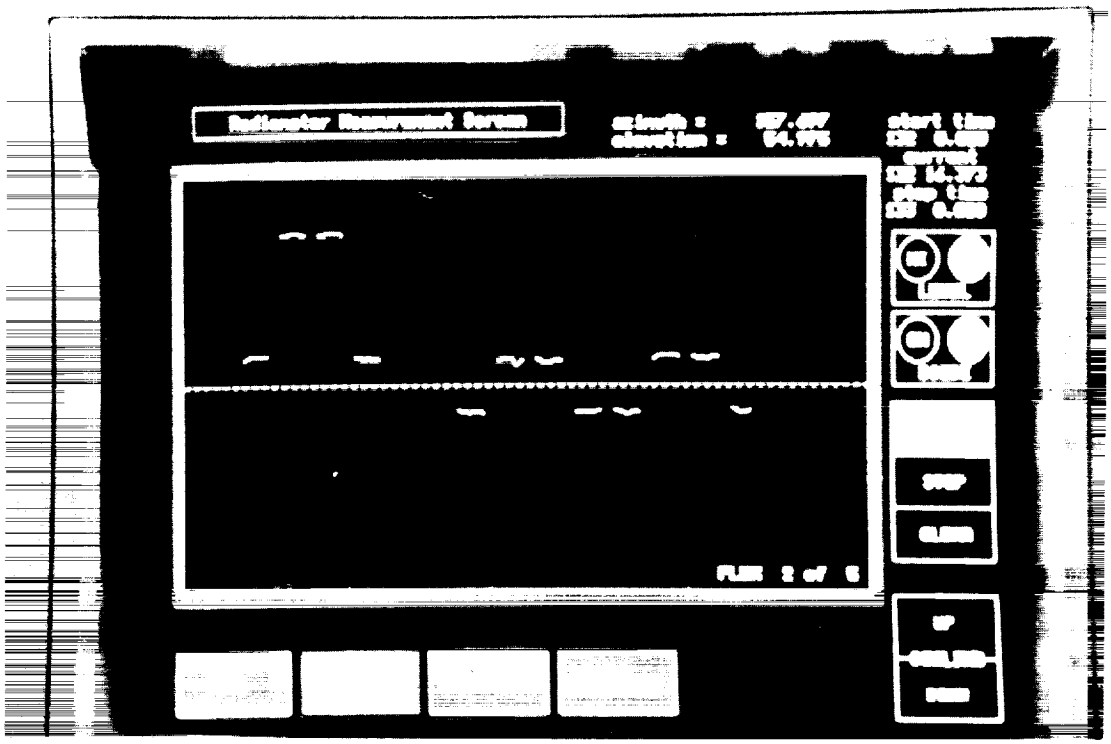

Fig. 19. Display picture of a flux measurement.

The diode measurement method is simple. While tracking, and with the antenna scanned off-source in azimuth, four power level measurements are made. These measurements are made with the diode power injected into horn A and for the diode turned off, on, on, and off. The sum of the diode-off power levels was subtracted from the sum of the diode-on power levels, and the result was divided by 2 to obtain an average diode power level. These four measurements were made in this manner in order to eliminate any error due to short-term variations in the receiver gain during the calibration sequence.

Drift Curves. Drift curves are of use in determining the performance of the antenna. These curves allow the observer to determine the beamwidth of the antenna and can be used in conjunction with other mathematical techniques to determine the source-size correction factors to apply to measurements of sources that are not extremely small with respect to the antenna beamwidth. For this article, the drift curve is used to verify the size of the antenna beams as measured by NIST. These data are taken by driving the antenna to a position that is in advance of the source. For this positioning system, an offset of the time "axis" (also known as hour angle) is allowed. Thus, driving the antenna ahead of the source by a set time and then setting the brakes allows the source to slowly (sidereal rate) drift through the antenna beam. Figure 20 shows the results of one drift curve done using Venus as the source. The beamwidth calculated by this curve is 0.430 deg, which is in very good agreement with the measurements.

V. Tracking System

A. Azimuth/Elevation Positioner System

The antenna is mounted on a Scientific-Atlanta elevation-over-azimuth positioner that has a range of 100 and 540 deg of rotation in the elevation and azimuth axes, respectively. Servo motors on each axis are driven by a model 3840 positioner controller from the same manufacturer. This controller accepts a

variety of commands from its front panel or a remote computer, reads the encoders on each axis of the positioner, and drives the antenna in response to these commands and indications. The 3840 also displays these commanded and indicated positions on its front panel and sends them to a remote computer.

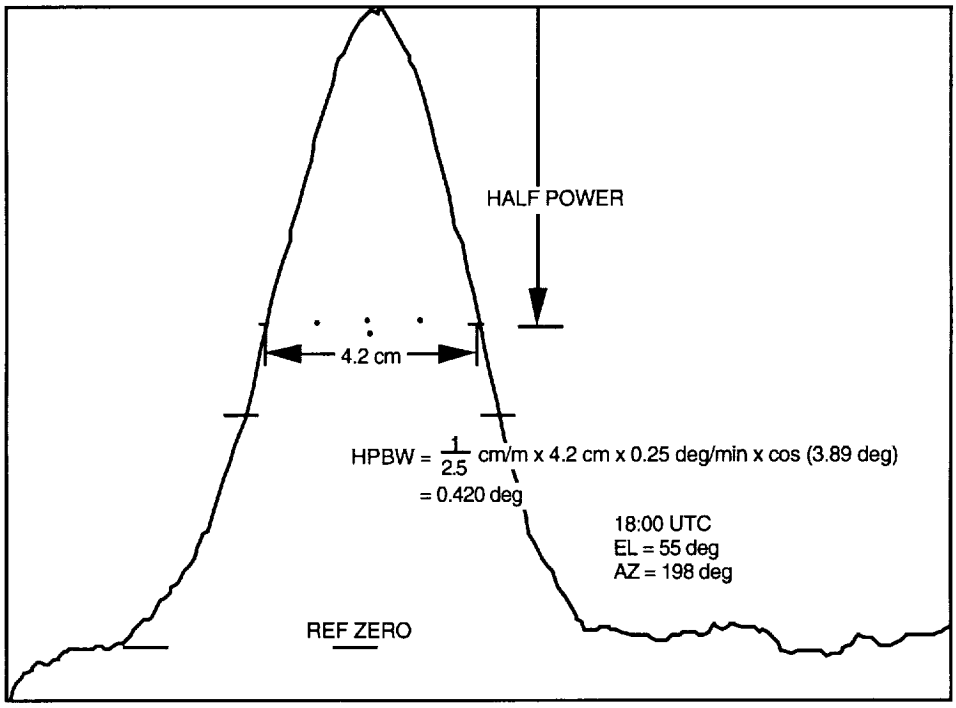

Fig. 20. Drift curve of beam A using Venus. Venus declination = 3.89 deg, April 29, 1983, chart speed = 2.5 cm/min.

The four active modes of this 3840 controller, which are available for this telescope, are stow, slew, position, and scan. In its stow mode, the controller drives the antenna servos at full rate to a zero position defined internally by user-selectable jumpers. In the slew mode, the antenna servos are driven at a variable rate in the direction selected by the user. In the position mode, the antenna servos are driven at a moderate tracking rate until the indicated position matches the commanded position. And in the scan mode, the antenna is driven to oscillate around the current position between user-defined limits at a user-defined rate. A fifth mode, standby, is used to disengage the drive motors and set the brakes on the positioner when tracking is done. It should be noted that no firmware exists in this controller to conduct antenna tracks in either sidereal or planetary mode; therefore, a remote computer is required to send continuous new commanded positions to conduct these tracks.

The remote computer used for tracking is a Hewlett-Packard Vectra 386 with a touch screen. This computer serves as a virtual device by displaying the equivalent of the 3840 controller's front panel on the screen, and through the use of the touch screen, it allows the user to activate any command button just as one would on the 3840 front panel. In addition, the user is also capable of scanning through several data-display and system-configuration screens on this computer. By way of touch screen and keyboard inputs, the experimenter may select the source to be tracked, the tracking mode to use, and the type of data collection to conduct.

B. Tracking Software

As stated above, the Scientific-Atlanta 3840 positioner controller cannot of itself conduct antenna tracks. It requires an external computer to continuously send new position commands. The software on

this computer must therefore be able to produce position commands for the necessary tracking modes. It was decided at the start of this project that two tracking modes were necessary, sidereal and planetary. Furthermore, there should be a capability to superimpose a scan on top of the tracking mode to perform secondary measurements. These requirements were met by a combination of software provided by the Scientific Atlanta as part of the delivery of the 3840 positioner controller and software added by JPL to perform specific boresighting and tracking capabilities common to JPL deep space tracking systems.

1. Tracking Modes. Sidereal. In the sidereal mode, the antenna tracks a radio source at a fixed right ascension (RA) and declination (DEC), and the antenna moves to compensate for the rotation of the Earth. The RA and DEC of the source to be tracked are supplied to the tracking software by the user. Although the user occasionally supplies these coordinates for the current day, they are usually retrieved from an ephemeris listing with coordinates at some past or future date which need to be corrected for the Earth's precession to the current date. For this reason, the software requires four inputs to conduct a sidereal track: the right ascension and declination, the epoch of the RA and DEC coordinates, and whether or not to apply precession correction. Once these values have been input, the computer will compute azimuth and elevation command positions.

Planetary. In the planetary mode, the antenna tracks a radio source at a variable RA and DEC, and the antenna moves to compensate for the rotation of the Earth and the motion of the source. In this mode, the user is required to supply three data sets consisting of a date and time and the RA and DEC of the source for that date and time. Through these three points, the computer fits a second-order curve. Using the current date and time and this curve, the computer then calculates the current RA and DEC of the source and calculates azimuth and elevation command positions from these coordinates. It should be noted that as the time between these three points increases, a significant error in the calculation of the current RA and DEC can result. Therefore, for this experiment, we consistently supplied coordinates that were only 6 hr apart.

2. Scanning Capability. In addition to the sidereal and planetary tracking modes that have been added to the positioner controller software, there are modes available that allow for scanning the antenna in elevation, azimuth, and in the time base (hour angle). These scan modes can be applied while the antenna is stationary or while it is tracking. This feature is useful in searching for targets upon initial acquisition. Prior to the development of pointing models for a particular part of the sky, a search may be made by superimposing a scan in any or all of the axes while observing a strip chart display of the detected signal. Another use of this capability would be to measure the antenna patterns or to measure source sizes in the development of non-point-source correction factors. This useful mode of operation is not widely used other than for initial source acquisition.

VI. Performance

The telescope has been assembled and was used in a side-by-side observation of Venus along with the OVRO 5-m antenna during the summer of 1993. During this period, the performance parameters of the system were calibrated, often many times. Table 4 summarizes all performance parameters measured during this period and their predicted values where a prediction was made. For completeness, the performance parameters measured at NIST are included in this table.

VII. Summary

A radio telescope has been developed and delivered to the field that can accurately measure the flux density of the brightest radio sources. This telescope uses an antenna system that has been calibrated to high absolute accuracy. The calibration matches well with the predicted performance for this system. This telescope uses a Dicke beam-switching radiometer that can provide 8-mK sensitivity in a 1-sec integration time. This radiometer is extremely stable and linear, and by virtue of its beam switching eliminates the

transitory effects of the atmosphere during observations. The calibration and supporting documentation suggest that this is the most highly accurate standard gain system for radiometric observations at 32 GHz yet reported. The system supported a set of side-by-side observations of Venus, the purpose of which was to determine very accurately both the gain of the associated telescope, an OVRO 5-m antenna, and the disk temperature of Venus. Those measurements were highly successful and will be reported in a future article.

Table 4. The 1.5-m telescope performance.

Parameter	Measured value	Predicted value
System noise temperature, K	75	75
Receiver temperature, K	65	65
Stability, dB/hr	0.06 (maximum)	–
Maximum blind pointing error, deg	0.022	0.030
Minimum ΔT (noise floor), mK	8	10
Separation of beams, deg		
Azimuth (NIST)	1.00	1.00
Azimuth (OVRO)	0.99	–
Elevation (NIST)	0.02	0.00
Elevation (OVRO)	0.02	–
Linearity, percent	99.2	–
Half-power beamwidth, deg		
NIST calibrations	0.430	0.43
OVRO calibrations	0.420–0.440	–

Acknowledgments

The principal author would like to thank his coauthors for their dedicated support during this multiyear development. Also, this system would not have been completed without the help of Dudley Neff, Richard Hodges, Manuel Esquivel, Gary Glass, Leon Alvarez, Hal Ahlstrom, Fred Menninger, Ron Heuerman, George Resch, and Rob Hartop of JPL, and Wil Klemperer and Andy Repjar of NIST.

References

[1] G. Evans, *RF Radiometer Handbook*, Dedham, Massachusetts: Artech House, 1977.

[2] N. Skou, *Microwave Radiometer Systems Design and Analysis*, Dedham, Massachusetts: Artech House, 1989.

[3] A. Cha, "An Offset Dual Shaped Reflector With 84.5 Percent Efficiency," *IEEE Transactions on Antennas and Propagation*, vol. AP-31, no. 6, November 1983.

[4] P. D. Potter, "A New Horn Antenna With Suppressed Sidelobes and Equal Beamwidths," *Microwave Journal*, vol. VI, no. 6, pp. 71–78, June 1963.

[5] A. J. Repjar, *Final Project Report, Calibration of the JPL 1.5 Meter Clear Aperture Antenna*, Report Number SR-723-61-90, National Institute of Standards and Technology, Boulder, Colorado, December 31, 1990.

[6] R. H. Dicke, "The Measurement of Thermal Radiation at Microwave Frequencies," *The Review of Scientific Instruments*, vol. 17, pp. 268–275, July 1946.

[7] J. Bowen and D. Neff, "A Cryogenic Seven-Element HEMT Front End for DSS 13," *The Telecommunications and Data Acquisition Progress Report 42-114, vol. April–June 1993*, Jet Propulsion Laboratory, Pasadena, California, pp. 51–60, August 15, 1993.

[8] C. T. Stelzried and M. J. Klein, "Precision DSN Radiometer Systems: Impact on Microwave Calibrations," *Special Issue of the IEEE Proceedings on Design and Instrumentation of Antennas for Deep Space Telecommunications and Radio Astronomy*, February 1994.

[9] C. T. Stelzried, *The Deep Space Network—Noise Temperature Concepts, Measurements, and Performance*, JPL Publication 82-33, Jet Propulsion Laboratory, Pasadena, California, September 15, 1982.

[10] M. S. Gatti, M. J. Klein, and T. B. H. Kuiper, "32-GHz Performance of the DSS-14 70-Meter Antenna: 1989 Configuration," *The Telecommunications and Data Acquisition Progress Report 42-99, vol. July–September 1989*, Jet Propulsion Laboratory, Pasadena, California, November 15, 1989.

[11] S. D. Slobin, W. V. T. Rusch, C. T. Stelzried, and T. Sato, "Beam Switching Cassegrain Feed System and Its Applications to Microwave and Millimeterwave Radioastronomical Observations," *The Review of Scientific Instruments*, vol. 41, no. 3, pp. 439–443, March 1970.

[12] A. C. S. Readhead, C. R. Lawrence, S. T. Myers, W. L. W. Sargent, H. E. Hardebeck, and A. T. Moffet, "A Limit on the Anisotropy of the Microwave Background Radiation on Arc Minute Scales," *The Astrophysical Journal*, vol. 346, pp. 566–587, November 15, 1989.

[13] "IRE Standards on Electron Tubes: Definition of Terms," 1962 (62 IRE 7.S2 IEEE Standard No. 161), *Proceedings of the IEEE*, March 1963.

[14] C. T. Stelzried, "Non-Linearity in Measurement Systems: Evaluation Method and Application to Microwave Radiometers," *The Telecommunications and Data Acquisition Progress Report 42-91, vol. July–September 1987*, Jet Propulsion Laboratory, Pasadena, California, pp. 57–66, November 15, 1987.